ISSN 1392-1207. MECHANIKA. Vol. 30, No. 6, 2024: 544–559

Enhancing Terrain Adaptability of Micro Tracked Chassis: A Structural Design and Performance Evaluation

Chang SU*, Hao HUANG**
**School of Mechanical Engineering, Anhui University of Science and Technology, 232001 Huainan, Anhui, P. R. China, E-mail: suchang_user@163.com*
***School of Mechanical Engineering, Anhui University of Science and Technology, 232001 Huainan, Anhui, P. R. China, E-mail: haohuang202202@163.com (Corresponding author)*
https://doi.org/10.5755/j02.mech.36883

1. Introduction

In recent years, advances in engineering have propelled the deployment of mobile robots in complex work environments, demanding capabilities in autonomous navigation, obstacle avoidance, and adaptive locomotion [1]. For traversing uneven, soft terrain or inclines, tracked robots offer superior ground contact and maneuverability compared to wheeled platforms [2]. However, conventional tracked designs struggle with ground tilt, increasing the risk of accidents [3]. The development of adaptive tracked chassis addresses these limitations, enabling robots with the ability to adapt to diverse mobility demands and maintain stability across challenging terrains. This innovation holds promise for a wide range of applications, including agricultural tasks in mountainous regions [4], computer vision-based crack detection in subway tunnels where the chassis can act as a stabilizing platform [5], subterranean mine exploration [6], seabed exploration [7], disaster relief involving material transport or organism detection in rugged environments [8], and even extraterrestrial missions [9]. These advancements significantly enhance robot adaptability, efficiency, and safety, broadening their utility across various domains. Consequently, research and development in adaptive tracked chassis are crucial for augmenting robot adaptability, flexibility, and safety, ultimately expanding their applicability across diverse sectors.

The adaptability of tracked chassis is crucial, given their diverse operational requirements. To address the challenge of self-adaptation, researchers worldwide have conducted extensive research, focusing particularly on enhancing the structural integrity of the chassis to bolster its traversability and stability. Li et al. [10] conducted a comprehensive analysis, developing a small crawler-based corn harvester that demonstrated robust adaptability to inclined terrain, thus enabling mechanized corn harvesting in hilly areas and significantly enhancing agricultural productivity. introduced Polibot, Ugenti et al. [11] innovated a novel off-road tracked robot equipped with a passive articulated suspension system, where each walking wheel is independently suspended to navigate irregular terrains with ease. In a separate study, Li et al. [12] engineered a wheel-rail composite chassis, featuring a crawler walking mechanism at the front wheel and a wheel-type walking structure at the rear. Through rigorous modeling and simulation using RecurDyn, they evaluated track tension and driving torque variations, validating the rational design and adaptability of the chassis.

In response to forest terrain challenges, Zhou et al. [13] devised a fish-bellied swing arm torsion bar suspension system based on robot kinematics and tracked vehicle suspension principles. By modifying the original shaft tube swing arm of a tracked forest fire truck to a fish-bellied swing arm and upgraded the semi-rigid shaft tube suspension to torsion bar suspension, they conducted static and dynamic simulations of the improved prototype vehicle. Their findings showcased that the fish-bellied swing arm torsion bar suspension system effectively mitigated swing arm bending moments, resulting in smoother vehicle operation and fulfilling forest transportation needs. Additionally, Bai et al. [14] developed a dynamic model of a robot in RecurDyn and constructed the robot model. Through simulation and prototype testing, they affirmed the robot's exceptional obstacle-surmounting capability and successful navigation through multi-level deformations, thereby validating the structural design's feasibility.

Several researchers have investigated body leveling theory for attitude adjustment in various applications. Wang et al. [15] proposed a body leveling control model that adapts to terrain characteristics. This model calculates real-time body posture and formulates corresponding control strategies. They also developed a leveling control model based on tire stiffness and tire mass displacement. Comparative analysis revealed an average pitch angle error of 7.94% and an average inclination angle error of 4.37%. Hu et al. [16] designed an adaptive leveling hydraulic suspension system by incorporating a load-sensing system into the hydraulics and control model. They further modeled and simulated the load-sensing system, providing theoretical support for similar adaptive leveling systems.

Focusing on rapid response, Wang et al. [17] presented a fast active leveling method. This method utilizes detection equipment to perceive ground information during vehicle motion and feeds it back to the control system. The actuator is then manipulated to execute the leveling mechanism, ensuring platform stability. Experimental results demonstrated that the fast active leveling system maintained platform pitch and roll angles within ±0.5° for over 80% of the testing period. Alexandr et al. [18] optimized the leveling system of logging machine platforms by converting hydraulic cylinder rod translation into a rotational mechanism. Three hydraulic cylinders facilitated effective longitudinal and transverse leveling. Their analysis supported the system's effectiveness in logging machine design.

For high-precision applications, Xiao et al. [19] developed a four-point support hydraulic leveling control system using a fuzzy PID control method with an STM32 single-chip microcomputer as the core. Experimental tests confirmed the system's superior control performance, high

leveling accuracy, and fast reaction time, meeting the demanding control requirements of radar vehicles. Finally, Yang et al. [20] proposed a three-degree-of-freedom suspension mechanism for tractor tools. This mechanism enables position and attitude adjustments through three active movements, facilitating automatic chassis leveling of tractors and farm tools on slopes.

Although the traditional track chassis has certain adaptability in complex terrain, it has obvious limitations in terms of flexibility, weight, real-time response ability, etc., especially when dealing with rugged, slippery or soft terrain, its trafficability and stability are often limited. These problems lead to the poor performance of existing technologies in practical applications such as agriculture, mining, and disaster relief. In view of the above problems, we have designed a miniature crawler chassis that can adapt to complex terrain to improve its flexibility, trafficability and stability.

The core issue of this study is to make the miniature crawler chassis more adaptable through innovative structural design and control algorithms, especially to maintain stability when dealing with various terrains such as ramps, ravines, and vertical obstacles. Compared with the existing solutions, our chassis not only has the ability to respond quickly to environmental changes, but also achieves accurate adjustment of the chassis posture through four independently controlled lifting mechanisms, so that it can maintain the best state in a variety of complex terrains.

In this study, a new type of micro-adaptive tracked chassis design is proposed and verified. Through structural optimization and dynamic modeling, the adaptability and trafficability of the tracked chassis in complex terrain are significantly improved. Through RecurDyn simulation and actual test, we verify the excellent performance of the chassis in a variety of complex scenarios, which provides new ideas and technical support for the design of mobile platforms in complex terrain.

2. Theoretical Analysis of the Trafficability of Miniature Crawler General Chassis

The theoretical calculation and analysis of the passing performance of the miniature track universal chassis under different terrain conditions are carried out, including longitudinal ramps, transverse ramps, trenches and vertical obstacles.

2.1. Performance analysis of climbing

2.1.1. Performance analysis: longitudinal ramp climbing

1. When a general chassis ascends vertically uphill at a constant speed, the force analysis diagram of the chassis on the longitudinal ramp is depicted in Fig. 1.

Where the longitudinal limit tipping angle is denoted as α_{lim1}, and the longitudinal slip angle is represented by α_{φ}. Additionally, L signifies the grounding length of the track in millimeters (mm), while b denotes the distance between the chassis center of mass and the rear wheel (mm), and a indicates the distance between the chassis center of mass and the front wheel (mm). The parameter h stands for the distance between the center of mass of agricultural machinery and the ground (mm), while n represents the ground reaction and rear wheel spacing (mm). N_1 indicates the vertical supporting force of the ground facing the track in Newtons (N), and F represents the resistance of the track to the ground (N). Moreover, O symbolizes the position of the chassis's center of mass, and G represents the chassis weight in Newtons (N).

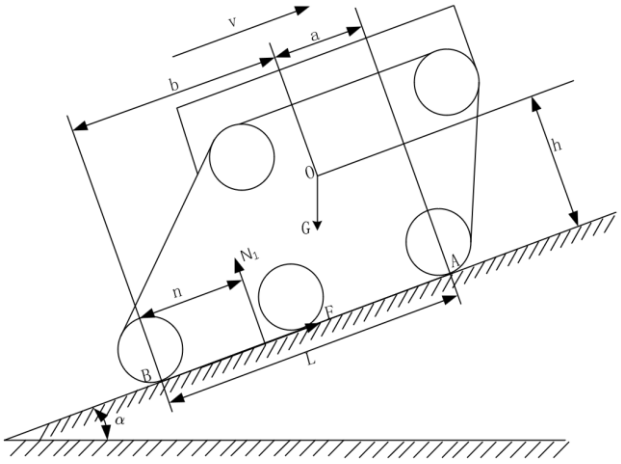

Fig. 1 Force analysis of chassis when uphill

As previously mentioned, when the chassis ascends at a constant speed, the influence of external factors is relatively minimal, resulting in the chassis being in equilibrium. In other words, the resultant force acting on the chassis is zero, leading to the equilibrium equation:

$$F - G\sin\alpha = 0, \tag{1}$$

$$N_1 - G\cos\alpha = 0. \tag{2}$$

Take the moment at point B:

$$N_1 n - bG_1\cos\alpha + hG_1\sin\alpha = 0. \tag{3}$$

According to the above:

$$n = \frac{b\cos\alpha - h\sin\alpha}{\cos\alpha}. \tag{4}$$

In order to prevent the chassis from tipping over during driving, it must satisfy the condition $n \geq 0$, where n represents the ground reaction force.

$$b\cos\alpha - h\sin\alpha \geq 0. \tag{5}$$

Therefore, we can derive the maximum tipping angle (α_{lim1}) of the miniature track universal chassis for stable climbing on a longitudinal slope as:

$$\alpha_{lim1} = arctan\left(\frac{b}{h}\right). \tag{6}$$

The maximum slip angle, denoted as $\alpha_{\varphi 1}$, for climbing along the slope is governed by the adhesion condition between the chassis track and the ground. The coefficient of adhesion between the road surface and the track component can be represented as φ. As the chassis maintains a constant speed on the ramp, it experiences balanced forces, leading to the following equilibrium equation:

$$F - G\sin\alpha_{\varphi} = 0, \tag{7}$$

$$N_1 - G\cos\alpha_\varphi = 0. \quad (8)$$

The adhesion of the chassis is $F_\varphi = \varphi N_1 = \varphi G\cos\alpha$, F_φ is the traction force generated by the chassis drive mechanism.

From this analysis, we can deduce that the condition for the chassis not to slip is represented by statement $F_\varphi \geq F$. Furthermore, the analysis reveals that the maximum slip angle of the chassis when driving on the ramp is denoted as $\alpha_{\varphi 1} = arctan\varphi$. As road conditions vary, the adhesion coefficient between the track and the ground also changes, consequently affecting the maximum slip angle. Generally, to ensure that the chassis does not tip over while driving on the slope, the maximum slip angle must be less than the maximum tip angle, denoted as statement $\alpha_{\varphi 1} \leq \alpha_{lim1}$. Hence, we can establish the relationship between the chassis parameters and the ground adhesion coefficient as statement: $\varphi \leq b/h$.

2. When a general chassis descends vertically downhill at a constant speed, the force analysis diagram of the tracked chassis on the longitudinal slope is illustrated in Fig. 2.

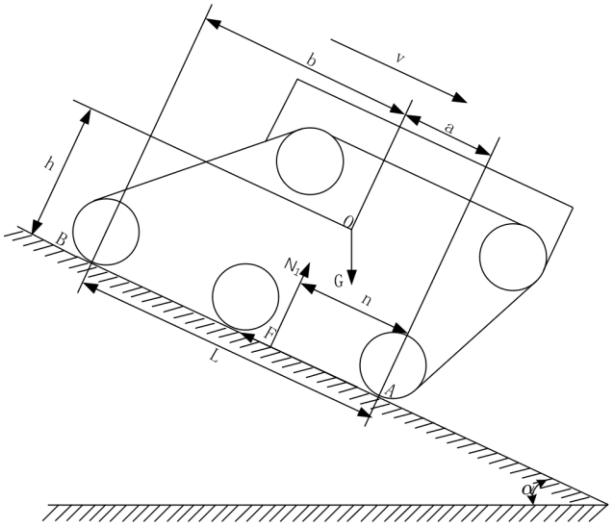

Fig. 2 Force analysis of the chassis on downhill slope

Where the longitudinal limit tipping angle at a constant speed downhill is denoted as α_{lim2}. Additionally, L represents the grounding length of the track in millimeters (mm), while b signifies the distance between the chassis center of mass and the rear wheel (mm), and a denotes the distance between the chassis center of mass and the front wheel (mm). The parameter h stands for the distance between the center of mass of agricultural machinery and the ground (mm), while n represents the ground support force and front wheel spacing (mm). N_1 indicates the vertical supporting force of the ground facing the track in Newtons (N), and F represents the resistance of the track to the ground (N). Moreover, O symbolizes the position of the chassis's center of mass, and G represents the chassis weight in Newtons (N).

Similarly, when $n \geq 0$, the chassis will not roll over. Therefore, the condition for preventing rollover can be expressed as $n \geq (a\cos\alpha - h\sin\alpha)/\cos\alpha$. Consequently, the maximum roll angle of the chassis that prevents rollover when descending downhill is $\alpha_{lim2} = arctan(a/h)$.

According to Fig. 3, it is evident that the primary factors influencing the slope angle α are the distance h from the center of gravity to the ground and the distances between the center of gravity and the front and rear wheels (a and b). Analysis indicates that when b remains constant, the slope angle α decreases with an increase in h. Conversely, when h remains constant, the slope angle increases with an increase in b. Theoretical analysis suggests that the maximum climbing angle is 36.87°.

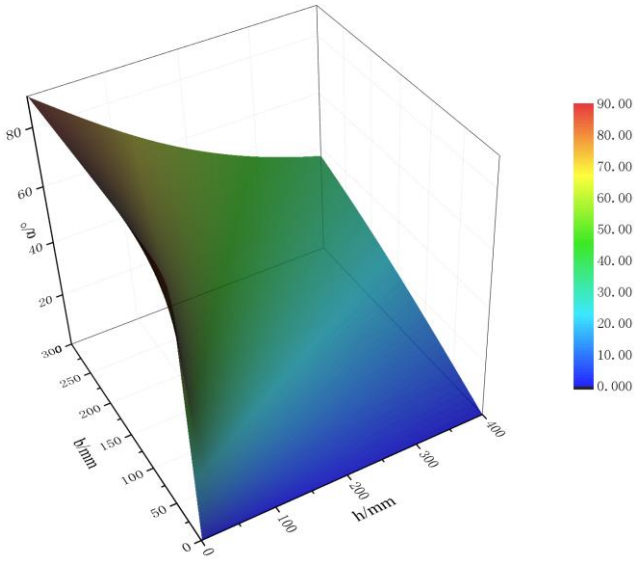

Fig. 3 The relationship between slope angle and chassis parameters

According to $\alpha_{\varphi 1} = arctan\varphi$, the maximum sliding angle under different ground properties can be obtained, as shown in Table 1.

Table 1
Maximum sliding Angle under different ground properties

Ground property	Ground adhesion coefficient φ	Maximum slip angle α, °
Earth highway	0.73	36.12
Gravel road	0.646	33.42
Soft sand	0.73	36.12
snowfield	0.45	26.5

It is imperative to ensure that the track chassis neither slips nor overturns when driving on the ramp, with the sliding angle always being smaller than the overturning angle. Based on the results presented in Table 1, it can be concluded that the chassis will not overturn when driving on the longitudinal ramp with various ground properties.

2.1.2. Transverse ramp through performance analysis

When the track chassis is operating at a constant speed on the lateral ramp, it is supported by the left and right tracks and is susceptible to slipping and tipping over. The force analysis is depicted in Fig. 4, where K represents the gauge in millimeters (mm). Additionally, n_2 denotes the distance between the pressure center of the track chassis and the center point C of the left track (mm), while N_2 and N_3 denote the supporting forces of the left and right tracks facing the ground in Newtons (N). The parameter t signifies the distance between the center of gravity and the longitudinal center axis of the track chassis (mm), and h_1 represents the distance from the center of gravity to the ground (mm).

The straight line represented by EF denotes the

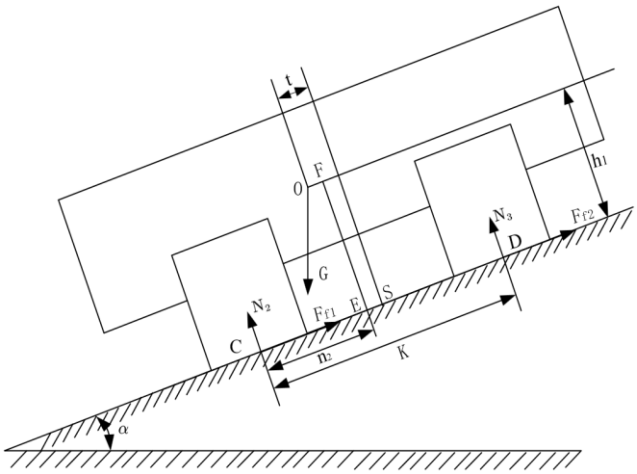

Fig. 4 Force analysis of the chassis when driving on a lateral ramp

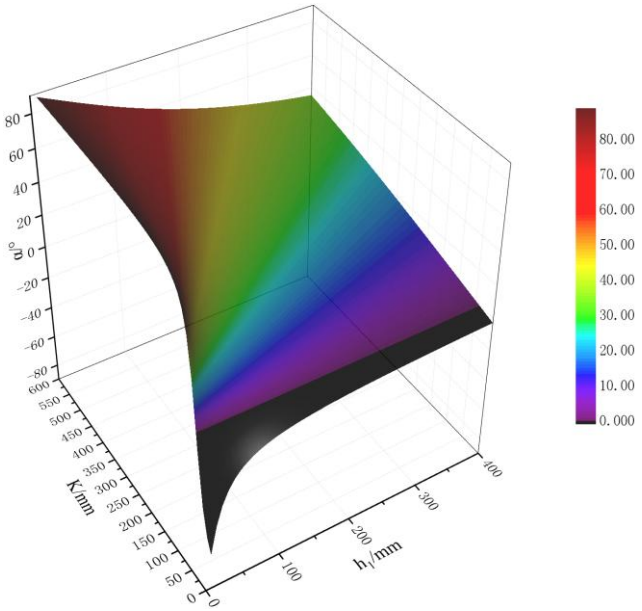

Fig. 5 Relation between slope angle and chassis parameters

center of gravity of the chassis pressure. As the slope angle increases, the pressure center will shift to the left, resulting in a decrease in n_2. When the pressure center moves to the left of point C, the chassis is prone to overturning.

The force analysis of the chassis yields the following insights:

$$F_{f1} + F_{f2} = G \sin\alpha. \tag{9}$$

$$F_{N2} + F_{N3} = G \cos\alpha. \tag{10}$$

Considering the moment acting about point C (as depicted in Fig. 4), we can derive the following equation:

$$h_1 G \sin\alpha - G \cos\alpha \left(\frac{K}{2} - t \right) + N_3 K = 0. \tag{11}$$

When tipping occurs, it implies that the supporting force on the right track, N_3, becomes zero. In this scenario, the maximum tipping angle can be determined:

$$\alpha_{lim3} = arctan\left[\left(\frac{K}{2} - t \right) / h_1 \right]. \tag{12}$$

The maximum slip angle α_φ of the chassis when driving on the lateral ramp is determined by the adhesion condition between the track and the ground. Lateral slip transpires when the chassis is navigating the lateral ramp. Hence, the occurrence of lateral slip must satisfy:

$$F_{f1} + F_{f2} \geq G \sin\alpha. \tag{13}$$

Therefore, $(F_{f1}+F_{f2})_{max} = \varphi G cos\alpha \geq G sin\alpha$. From this, it can be concluded that the maximum slope angle of the chassis without slipping is:

$$\alpha_{lim4} = arctan\,\varphi. \tag{14}$$

From the analysis, it is evident that the lateral stability of the chassis is primarily influenced by factors such as the center of gravity of the chassis, the gauge, and the ground condition. As illustrated in Fig. 5, theoretically, the maximum slope angle of the chassis when driving on a lateral ramp is 34.99°. To achieve optimal lateral stability, it is advisable to minimize the height of the center of gravity of the track chassis and the distance between the center of gravity and the central axis, while maximizing the gauge. The maximum slope angle for lateral sliding is identical to that of longitudinal sliding. However, since the maximum slope angle for lateral driving is 34.99°, it surpasses the maximum tipping angle for lateral driving. Nonetheless, the maximum sliding angle for soil and sand ground is greater than the maximum tipping angle for lateral driving, although they are similar. Consequently, theoretically, the chassis will neither tip nor slide at approximately 34° when driving on a transverse ramp.

2.2. Trench performance analysis

The trench is a common obstacle encountered during driving, serving as a crucial indicator for evaluating the passing performance of the crawler chassis. The width of the ditch that the crawler chassis can navigate through is contingent upon factors such as the length of the chassis grounding, the weight and center of gravity of the chassis, and the support force at both ends of the crawler. Consequently, it is essential to analyze the positional relationship between the center of gravity of the crawler chassis and the support points of the front and rear wheels when traversing the ditch.

Fig. 6 depicts various stages of the crawler chassis during trench traversal.

From the preceding analysis, it becomes apparent that the maximum width that the track chassis can traverse across the trench is primarily determined by the horizontal distance between the support points of the front and rear ends of the track and the center of gravity of the chassis in the driving direction. During the crossing of the trench by the track vehicle, the front end of the vehicle leaves the ground first. In this process, only after the front end of the track makes contact with the ground does the center of gravity of the vehicle leave the trench wall, allowing the track chassis to successfully traverse the trench. To ensure that both the front and rear of the track chassis remain clear of

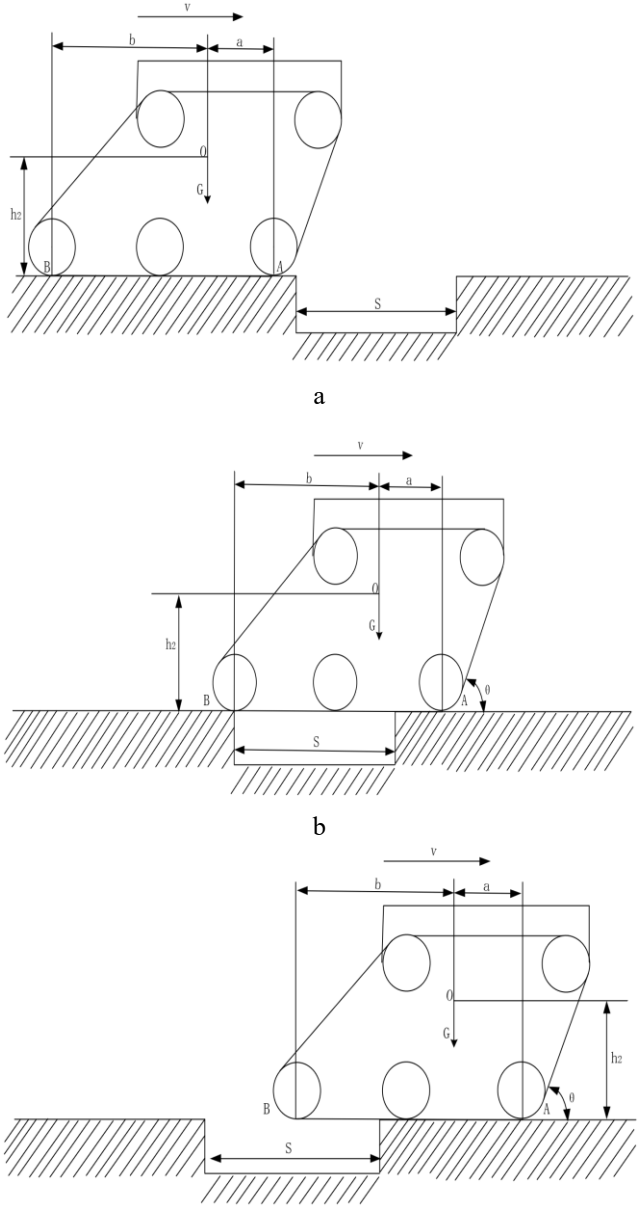

a

b

c

Fig. 6 The process of chassis crossing the trench: a – close to the trench, b – trench crossing, c – cross the trench

the trench while crossing, it is imperative to analyze the vehicle's state when entering and exiting the trench.

The analysis of the tracked vehicle crossing the trench, as depicted in Fig. 7, involves the trench width denoted as S_1 and S_2 in millimeters (mm). Additionally, a represents the distance between the center of gravity and the front wheel of the load-bearing wheel (mm), while b signifies the distance between the center of gravity and the rear wheel of the load-bearing wheel (mm). Furthermore, h_2 stands for the distance between the center of gravity and the ground (mm), and the slope angle θ is 20°. The maximum width across the trench can be determined through this analysis

$$S_1 = a + h_2 \tan\theta, \tag{15}$$

$$S_2 = b - h_2 \tan\theta, \tag{16}$$

$$S = min\left(S_1, S_2\right). \tag{17}$$

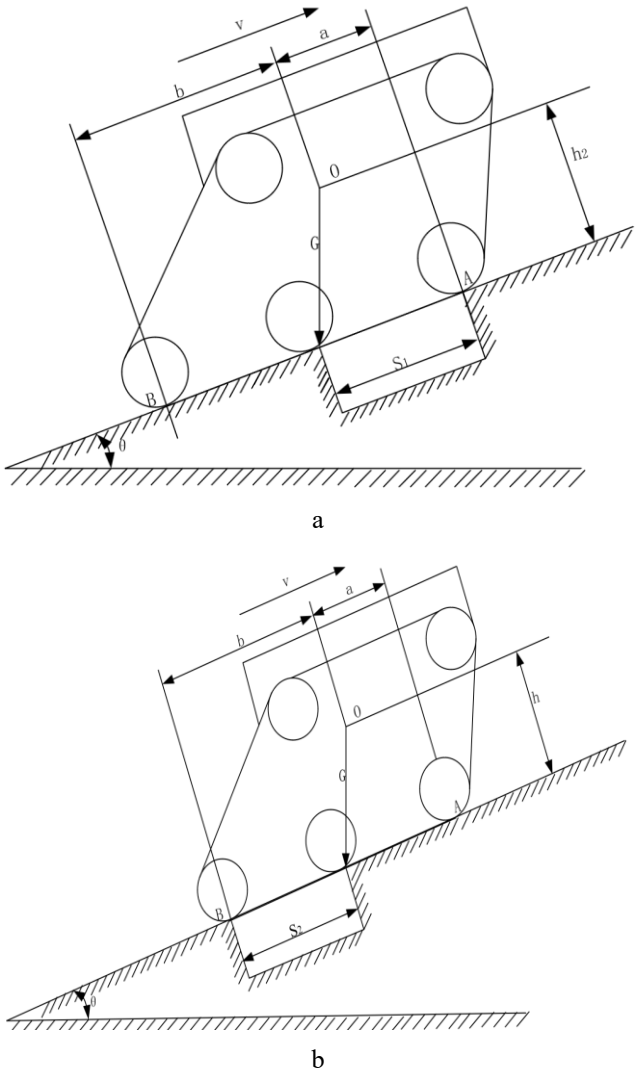

a

b

Fig. 7 Analysis of crossing the trench when uphill: a – crossing the trench position 1, b – crossing trench position 2

Based on the analyses presented in Eqs. (15), (16), and (17), the correlation between the trench width, slope angle, and the distances from the center of gravity to the front and rear wheels can be established. As depicted in Fig. 9, it is determined that the maximum trench width that can be traversed at a slope angle of 20° is 422 mm.

Through analysis, it is observed that in the initial stage of ditch-crossing, as depicted in Fig. 8, a, the width of the trench, denoted as S_1, increases with the augmentation of both a and h_2. Essentially, in the vicinity of the trench, a rearward movement of the chassis' center of gravity correlates with an enhanced capability of the chassis to traverse the trench.

Conversely, in the subsequent stage illustrated in Fig. 8, b, the width of the trench, labeled as S_2, enlarges with the escalation of both b and h_2. Thus, during the trench-crossing stage, a forward movement of the center of gravity strengthens the chassis' ability to traverse the trench. However, it's noteworthy that the influence of the working environment (such as slope angle and soil conditions) and chassis structure imposes limitations on the extent to which improvements in a, b, and h_2 can enhance the trench-crossing capability.

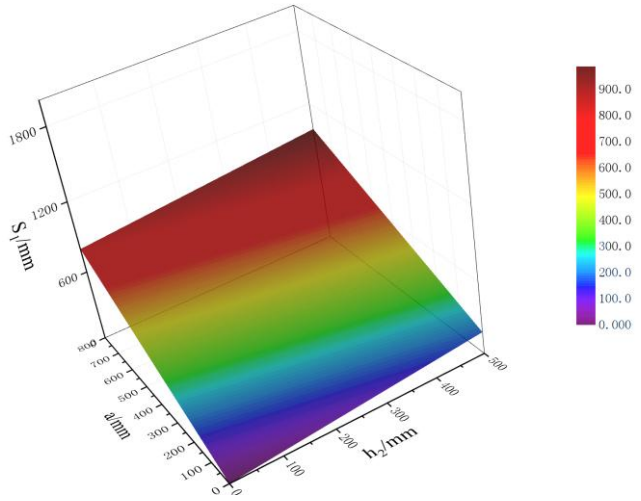

a

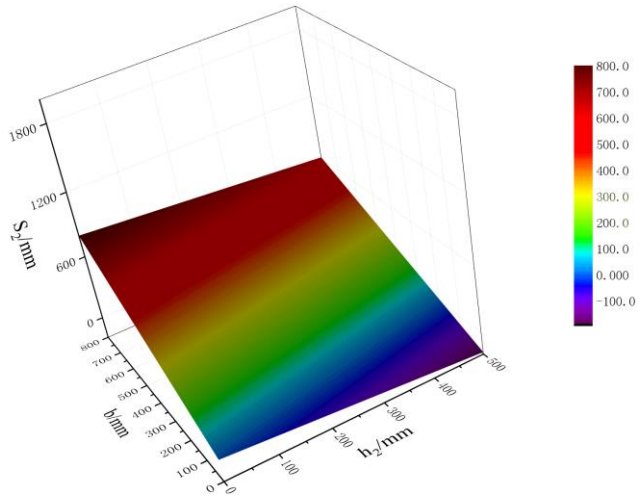

b

Fig. 8 The relationship between chassis size and trench width: a – the relationship between trench width and a and h_2, b – the relationship between trench width and b and h_2

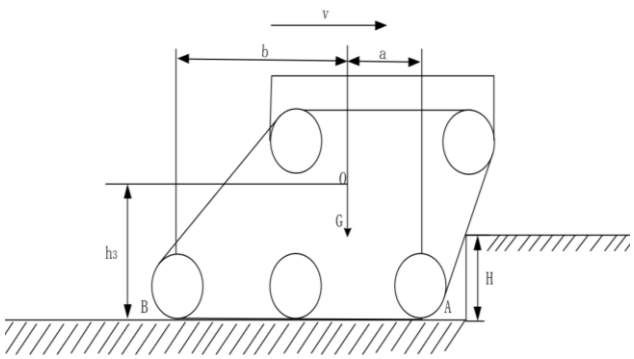

a

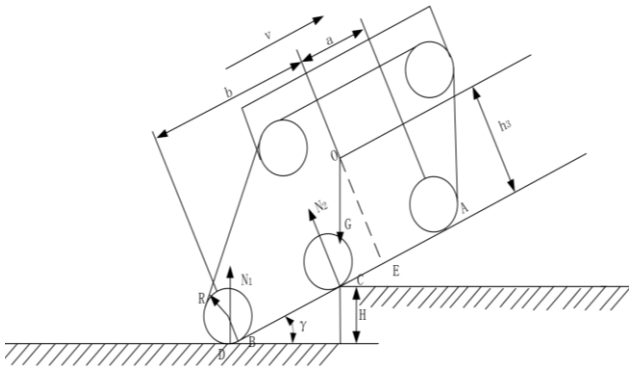

b

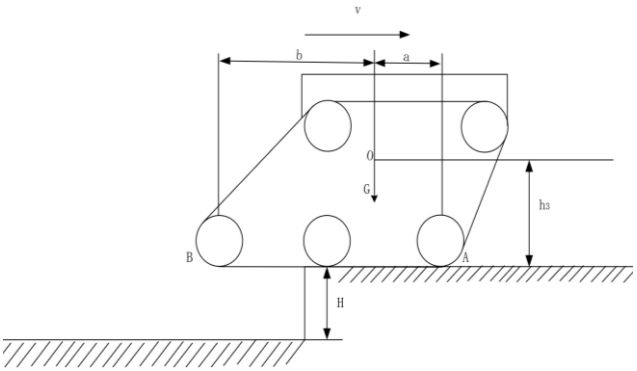

c

Fig. 9 Vertical obstacle crossing process of chassis: a – close to vertical obstacle, b – climbing vertical obstacle, c – crossing the vertical obstacle

2.3. Vertical barriers through performance analysis

When operating in a complex environment, a variety of obstacles may be encountered, with vertical obstacles being particularly common. Additionally, crossing vertical obstacles serves as a test for the chassis' obstacle-crossing ability. The process of crossing vertical obstacles typically involves three stages, as illustrated in Fig. 9.

When the track chassis reaches the critical state during the second stage of crossing the vertical obstacle, its ability to traverse the obstacle is influenced by the position of the center of gravity and the structural parameters of the chassis. As depicted in Fig. 9, b, when the crawler chassis enters the critical state of obstacle crossing, it reaches the maximum height for crossing the vertical obstacle. At this juncture, the vertical line passing through the center of gravity coincides with the edge of the vertical obstacle, indicating that the chassis is inclined towards crossing at point C. Consequently, the rear end of the track will detach from the ground, causing the chassis to rotate clockwise as a whole, ultimately resulting in a fall at the top of the vertical obstacle.

In Fig. 9, γ denotes the angle between the track and the ground, while H represents the height of the vertical barrier in millimeters (mm). Point C signifies the contact point between the chassis and the vertical obstacle. Additionally, N_1 represents the supporting force of the ground acting on the rear wheel of the track in Newtons (N), and N_2 denotes the support force of the vertical obstacle on the chassis in Newtons (N). Moreover, h_3 represents the vertical distance from the chassis' center of gravity to the ground in millimeters (mm), while a and b denote the distances from the center of gravity to the front and rear wheels, respectively, in millimeters (mm).

Through the analysis, it is evident that the relationship between the height of the vertical obstacle and the structural parameters of the general tracked chassis is as follows:

$$H = \left(b - h_3 \tan\gamma\right)\sin\gamma + \left(R - R\cos\gamma\right). \tag{18}$$

Take the moment of point B:

$$N_2\left(b-h_3\tan\gamma\right)-Gb\cos\gamma+Gh_3\sin\gamma=0. \quad (19)$$

When $N_2=0$, the pitch angle of the chassis reaches its maximum, so:

$$\gamma_{max}=arctan\left(b/h_3\right). \quad (20)$$

In the second stage of the track chassis, the center of gravity will continue to rise as the chassis continues to move, but two scenarios may occur based on the two cases described.

If the center of gravity of the track chassis continues to rise but remains in front of the vertical obstacle without passing its wall, the chassis may tip backward due to the excessive angle between the chassis and the ground.

However, if the center of gravity of the chassis continues to rise and exceeds the height of the vertical obstacle, causing the chassis to rotate clockwise, then the chassis can successfully cross the obstacle.

From these scenarios, it can be inferred that the angle between the chassis and the ground should not exceed 36.87° when crossing the obstacle. If this condition is violated, the chassis may tip over. Only when this condition is met can the chassis smoothly overturn and cross the obstacle.

As depicted in Fig. 10, the obstacle height that the tracked chassis can surmount increases with the angle between the chassis and the ground, reaching a relatively stable state after a certain threshold. Conversely, as the distance between the track's center of gravity and the ground increases, the chassis' capability to overcome vertical obstacles decreases. Thus, it is evident that a higher center of gravity of the track chassis is detrimental to obstacle traversal, while a lower center of gravity is advantageous. However, due to structural constraints, the angle between the track and the ground cannot consistently increase, nor can the distance between the center of gravity of the track chassis and the ground always decrease.

According to the analysis presented in Fig. 11, theoretically, when the pitch angle is 36.87°, the maximum obstacle crossing height of the crawler chassis is 170 mm. Nevertheless, exceeding this pitch angle may lead to overturning and slipping. Considering various operational conditions, the actual height of the crawler chassis when crossing vertical obstacles is limited to $H < 170$ mm.

3. Simulation Model Establishment

3.1. Basic structure

The 3D model of the micro crawler general chassis with adaptive terrain capability is presented in Fig. 12. This chassis consists of a main frame, four lifting mechanisms, drive wheels, support rollers, tensioning wheels, a diesel engine, inertial measurement units for attitude sensing, and an electronic control system.

3.2. Design of main parameters

Following the analysis of the miniature tracked chassis performance across various terrain conditions and considering practical application scenarios, the design specifications for the miniature tracked universal chassis have been formulated. The primary parameters of the tracked chassis are summarized in Table 2.

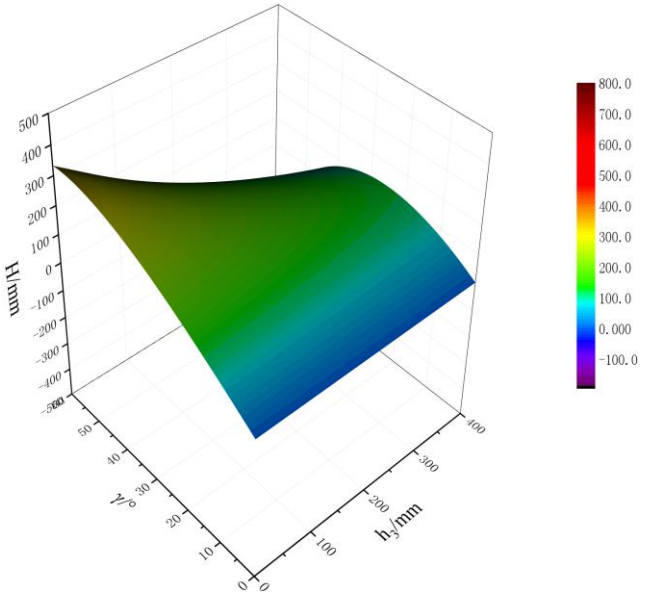

Fig. 10 Relationship between chassis structure parameters and vertical obstacle height

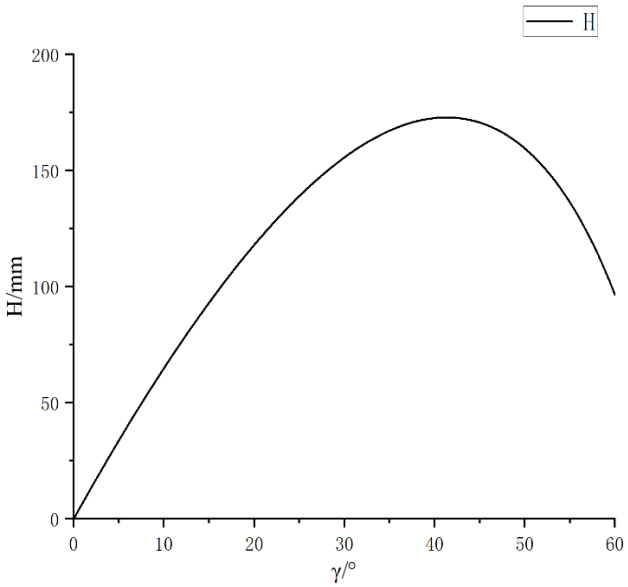

Fig. 11 Schematic diagram of limit obstacle crossing size

3.3. Principle of attitude adjustment

As shown in Fig. 12, b, the track chassis primarily achieves attitude adjustment through a lifting mechanism comprising hydraulic cylinders, rocker arms, swivel arms, and auxiliary arms. This mechanism is subdivided into four components: left front, right front, left back, and right back, each independently controlled. The extension and retraction of hydraulic cylinders actuate the rocker arms, which, in turn, drive the rotation of the swivel arms, resulting in displacement variation between the frame and the walking beam. Simultaneous lifting of both sides of the mechanism allows for chassis gap adjustment, facilitating angle adjustment. Furthermore, the control system can manipulate the chassis' center of gravity positioning in scenarios such as climbing and obstacle negotiation, significantly enhancing chassis traversal capabilities. Particularly on uneven road

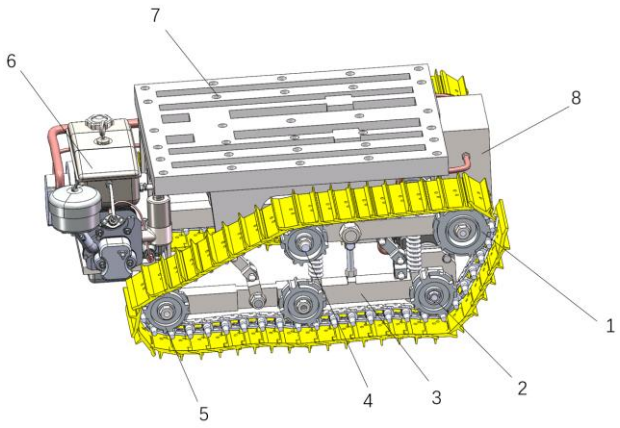

a

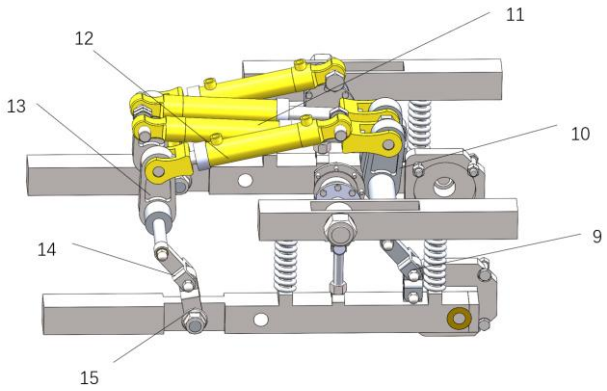

b

Fig. 12 Overall structure of miniature tracked chassis: a – chassis structure; b – lift composition: *1* guide pulley, *2* driving wheel, *3* walking beam, *4* bearing roller, *5* tensioning wheel, *6* diesel engine, *7* frame, *8* hydraulic and electronic control device, *9* front swivel arm, *10* front rocker arm, *11* front hydraulic cylinder, *12* rear hydraulic cylinder, *13* rear rocker arm, *14* rear swivel arm, *15* auxiliary arm

Table 2

Main design parameters of the general chassis of micro-track

Parameter	Numerical value
Chassis weight, kg	150
Maximum load weight, kg	50
Chassis length, mm	910
Chassis width, mm	600
Chassis height, mm	420
Track gauge, mm	350
Grounding length of the track, mm	730
Ground clearance, mm	150
Theoretical operating speed, km/h	0~5
Track width, mm	180
Track pitch, mm	72
Stiffness coefficient, kN/m	200
Stiffness coefficient	1

surfaces, this system ensures optimal traversal performance and driving stability.

3.4. Establishment of geometric model

Using the RecurDyn V9R4 released in China on June 1, 2021, when the RecurDyn software Track LM low-speed track module is used to build the virtual prototype of the track chassis, it is usually necessary to simplify the chassis. The frame, diesel engine and hydraulic pump are combined into a rigid body. At this time, the chassis can be simplified as the main body, four lifting mechanisms and track walking mechanism. The lifting mechanism includes a hydraulic cylinder, a rocker arm, a rotary arm and an auxiliary connecting rod. Each side walking mechanism includes a track, two sprockets, a drive wheel, a tension wheel and a supporting wheel. The institutions are constrained as shown in the following Table3.

Table 3

Constraint relationship of each component

Basal body	Movable body	Constraint type
Walking beam	Driving wheel	Revolution
Walking beam	Tension pulley	Revolution
Walking beam	Bearing roller	Revolution
Walking beam	Bearing wheel	Revolution
Rear rocker arm	Rear swivel arm	Revolution
Rear swivel arm	Auxiliary arm	Revolution
Rear rocker arm	Hydraulic cylinder	Revolution
Hydraulic cylinder	Hydraulic rod	Translation
Hydraulic rod support	Frame	Revolution

Due to the Track_LM module of Recurdyn software, it is not necessary to set the contact force and friction force on the ground. The results of setting four damping springs are shown in Fig. 13. The whole machine assembly drawing is shown in Fig. 14.

In order to make the chassis work, it is necessary to add the driving function to the crawler walking mechanism and the lifting mechanism, and select the STEP function as the driving function

$$STEP\left(x,x_0,h_0,x_1,h_1\right). \tag{21}$$

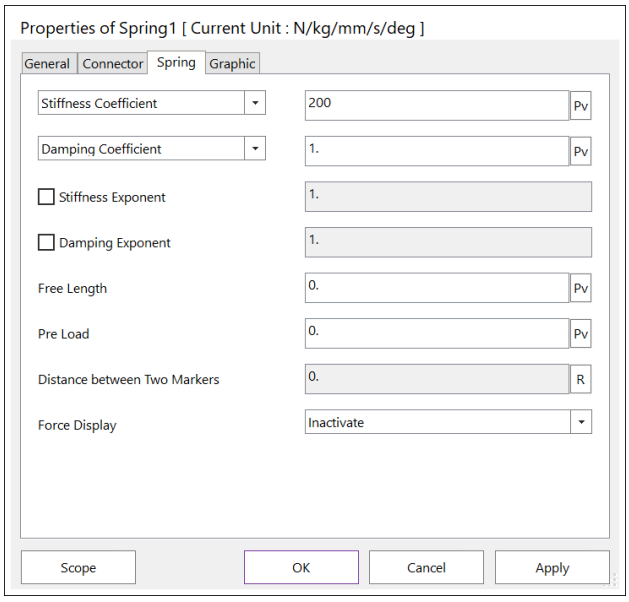

Fig.13 Spring force setting

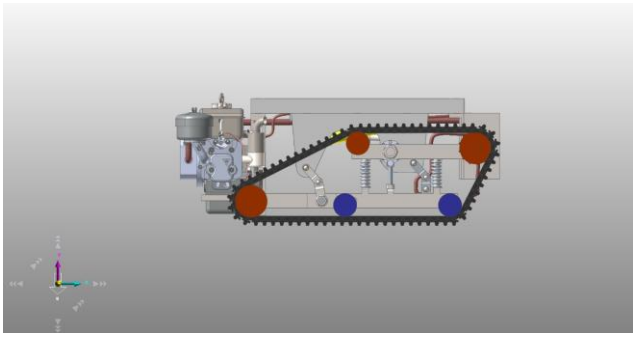

Fig.14 Overall dynamic modeling of crawler chassis

In the formula: x is the independent variable, select time as the independent variable; x_0 and x_1 are the initial value and the termination value of the independent variable respectively, that is, the time of the start and end of the simulation, and the values of x_0 and x_1 are changed according to the different contents of the simulation. h_0 and h_1 are the initial and final values of the design variables.

The 3D model was imported into RecurDyn, where various scenarios were simulated to replicate different terrain conditions, including sandy, clay, and heavy clay pavements. Table 4 provides the specific parameters corresponding to each type of pavement.

Table 4

Pavement parameters

Serial number	Soil parameter	Sandy pavement	Clay pavement	Heavy clay pavement
1	Deformation modulus of soil cohesion, Pa	0. 041861	0.4171	5.1737
2	Deformation modulus of friction force in soil, Pa	0. 012034	0.021888	0.63386
3	Deformation index	0. 7	0.5	0.13
4	Cohesion, N	0. 00172 0	0.00414	0.0685
5	Shear angle, °	29	13	34
6	Horizontal shear modulus, mm	25	25	25
7	Subsidence rate, %	5	3	5

4. Simulation Analysis of the Passability and Stability of the General Chassis with Track

The performance of the tracked chassis is influenced by several factors including the structural parameters of the chassis, soil conditions, traveling speed, and the position of the center of gravity when navigating through diverse environments. Through simulation and analysis using RecurDyn software, the tracked chassis is evaluated for its performance in uphill and downhill traversal, lateral movement, trench crossing, and obstacle negotiation.

4.1. Simulation analysis of driving performance at different gradients

4.1.1. Longitudinal climb simulation analysis

The climbing ability serves as a crucial performance metric for assessing the adaptability of the tracked chassis in complex environments. It gauges the chassis' capacity to ascend the steepest incline at a constant velocity without tipping over. Climbing ability is influenced by soil composition, driving velocity, and the positioning of the center of gravity. Utilizing RecurDyn, simulations of the tracked chassis are conducted under varying slope angles (15°, 25°, and 35°) across sand, clay, and heavy clay surfaces, as depicted in Fig. 15. Through these simulations on diverse ramps and surfaces, data including centroid velocity and centroid pitch angle are gathered, and subsequently fitted to generate Figs. 16, 17, and 18. The angular velocity driving function STEP (time, 0.1,0,1.5, -10) is added to the driving wheel at different slopes. The displacement driving function STEP (time, 0.1,0,4,80) + STEP (time, 4,0,8,-80) is set for the hydraulic cylinders of the two lifting mechanisms on the front side, and the displacement driving function STEP (time, 0.1,0,4,-80) + STEP (time, 4,0,8,80) is set for the hydraulic cylinders of the two lifting mechanisms on the back side. The simulation time is set to 8s, and the number of steps is 5000 steps.

The analysis presented in Figs. 16, 17, and 18 highlights the micro crawler chassis' remarkable stability during uphill climbs. Notably, the chassis maintains a near-parallel orientation relative to the slope throughout the ascent, signifying its robust adaptive capabilities. This stability is evident across all three investigated terrains (sandy soil, clay, and heavy clay), with the chassis demonstrating smooth ascents on each surface as the slope angle increases. However, the figures also reveal a trend in ascent velocity. Sandy soil exhibits the highest ascent speed, followed by clay and then heavy clay. This can be attributed to the differing mechanical properties of the terrains. Clay and particularly heavy clay exhibit plastic deformation and soil flow, which essentially reduces the grip and load-bearing capacity experienced by the chassis wheels. Consequently, the tracked chassis encounters a higher traction force requirement on these softer terrains, leading to a decrease in ascent velocity.

4.1.2. Transverse ramp driving simulation analysis

When the track chassis traverses a transverse slope, it becomes susceptible to tipping and slipping due to the slope's influence. Consequently, simulations were conducted using RecurDyn to assess the stability of the track chassis under various slope angles (15°, 25°and 30°) on sandy, clay, and heavy clay roads. Fig. 19 illustrates the outcomes of these simulations. The angular velocity driving

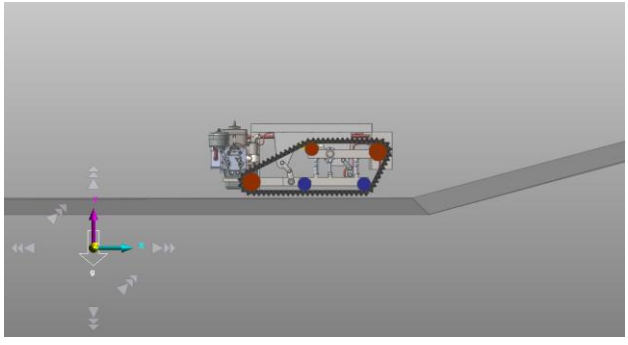

Fig. 15 Simulation analysis of chassis longitudinal climb

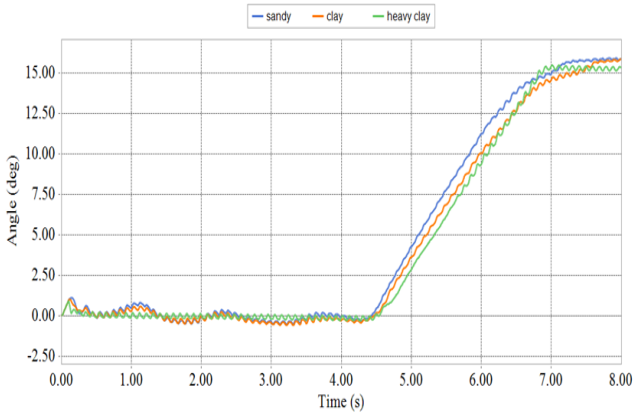

a

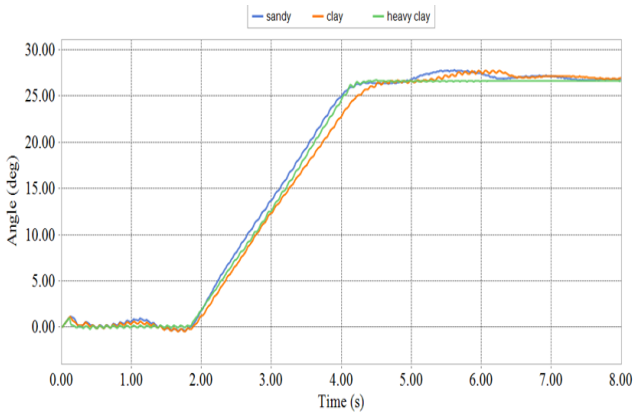

b

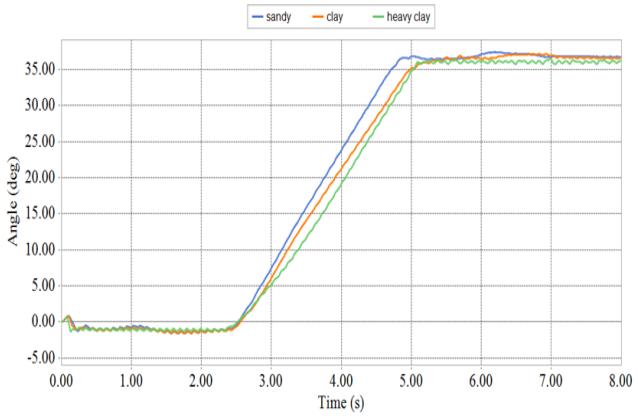

c

Fig. 16 Centroid pitch diagram of the chassis at different climbing angles: a – 15°, b – 25°, c – 35°

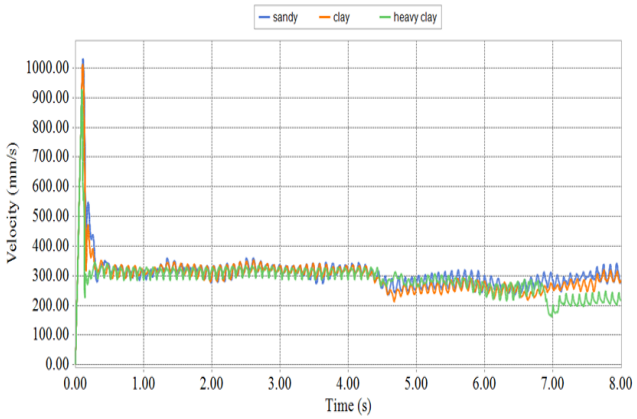

a

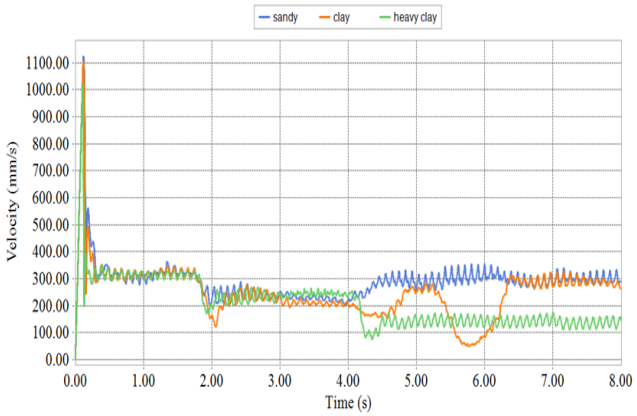

b

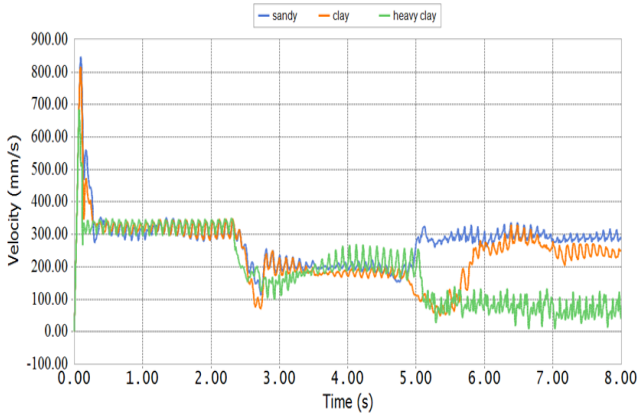

c

Fig. 17 Center of mass velocity of the chassis at different climbing angles: a – 15°, b – 25°, c – 35°

function STEP (time, 0.1, 0, 1.5, -12) is added to the driving wheel on different slopes, and the displacement driving functions STEP (time, 0.1, 0, 5, 80) and STEP (time, 0.1, 0, 5, -80) are set for the left and right hydraulic cylinders, respectively. The simulation time is set to 5 s and the number of steps is 3000 steps.

From Figs. 20, 21, and 22, it is evident that the tracked chassis exhibits relatively minimal and stable roll angles when traversing the transverse ramp, particularly on sandy terrain, demonstrating its stability during traversal. Although the roll angle increases with steeper slope angles, the chassis can still navigate the transverse ramp smoothly. Notably, on different road surfaces, the roll angle fluctuates more on clay and heavy clay terrain compared to sandy terrain, especially pronounced at a 30° slope angle. At a 15° incline, the centroid speed remains relatively steady, yet exhibits increased fluctuations with steeper slopes, particularly notable at a 30° incline. Generally, speeds are lower on sandy terrain compared to clay and heavy clay, with relatively stable speeds observed on sandy terrain. However, when traversing lateral slopes, a slight downward deviation is observed. Fig. 22 illustrates that this deviation increases with slope steepness, varying across different road surfaces. Significantly, the deviation on sandy terrain is notably smaller than that on clay and heavy clay surfaces. Overall, the chassis can traverse a 30° lateral ramp, but significant slipping and tipping occur beyond this threshold.

4.2. Simulation analysis of trench trafficability

The trench-crossing capability of the track chassis denotes its capacity to traverse a trench at a consistent speed without tipping over. Typically, the trench's navigability is correlated with soil type, trench width, track chassis speed, and the center of gravity's position. To assess this capability, RecurDyn simulations were conducted with trenches of varying widths (100 mm, 200 mm, 300 mm, 400 mm and 422 mm) on sandy, clay, and heavy clay pavements, all with a depth of 200 mm. Fig. 23 depicts the simulation setup. For the continuous crossing trench, the angular velocity driving function of the added wheel is STEP (time, 0.1,0,1.5, -10), the simulation time is 16 s, and the number of steps is 20,000 steps.

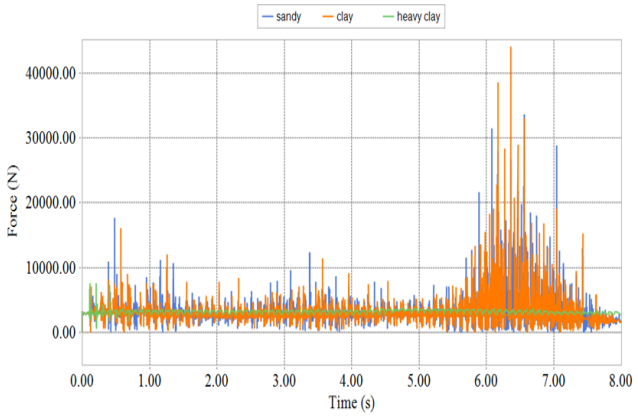

a

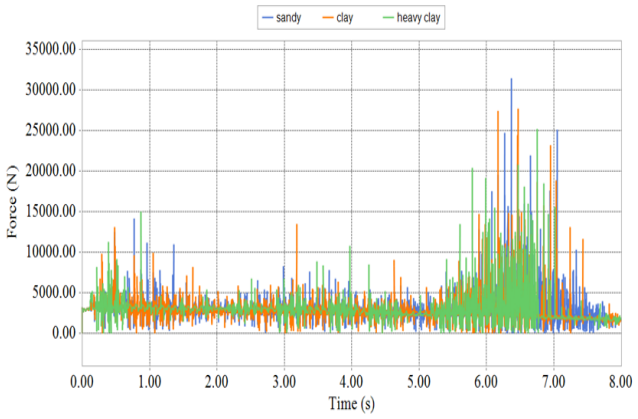

b

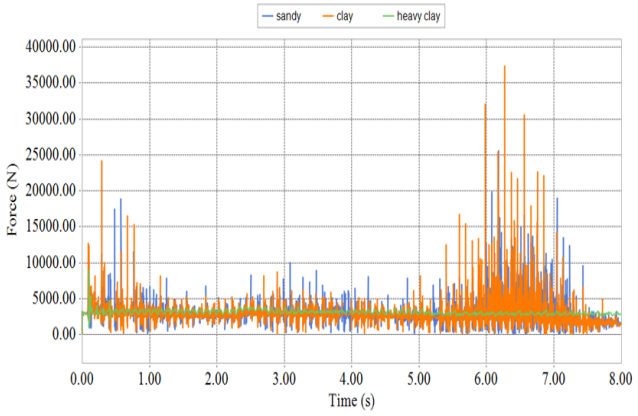

c

Fig. 18 Load bearing wheel on different ramps: a – 15°, b – 25°, c – 35°

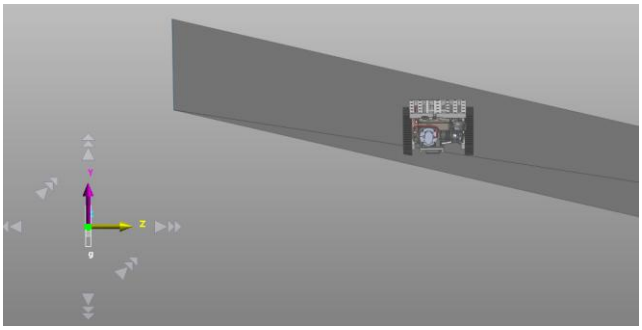

Fig. 19 Chassis driving on transverse ramp

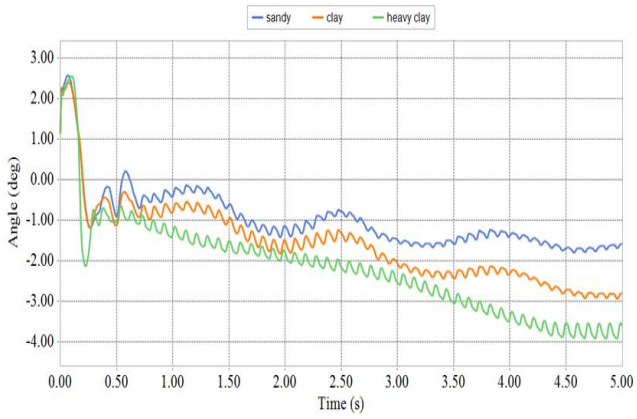

a

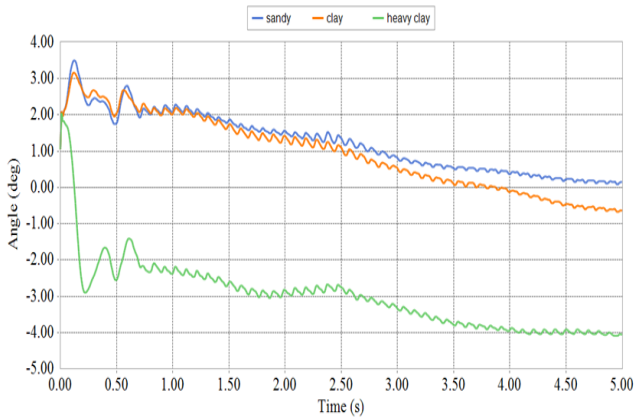

b

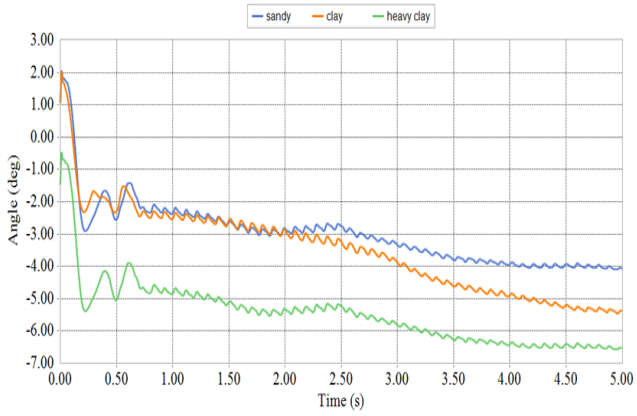

c

Fig. 20 Roll angle diagram: a – 15°, b – 25°, c – 30°

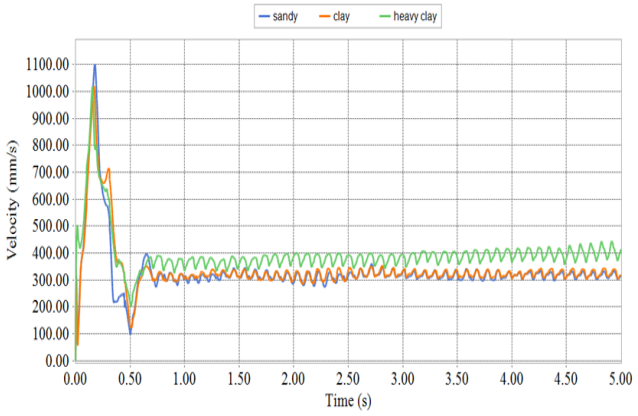

a

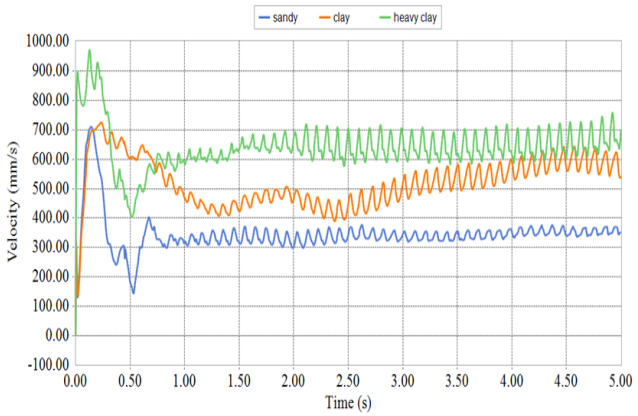

b

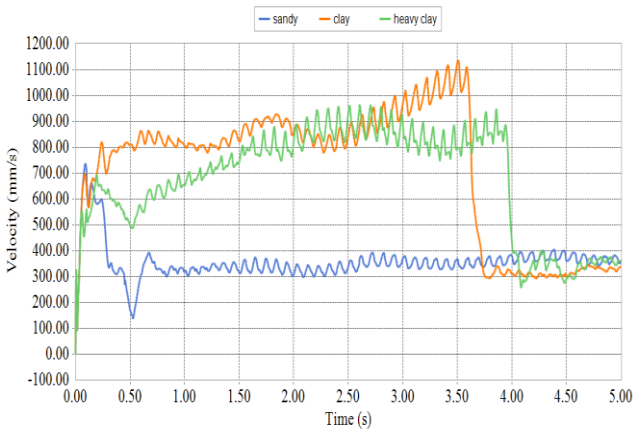

c

Fig. 21 Centroid velocity diagram: a – 15°, b – 25°, c – 30°

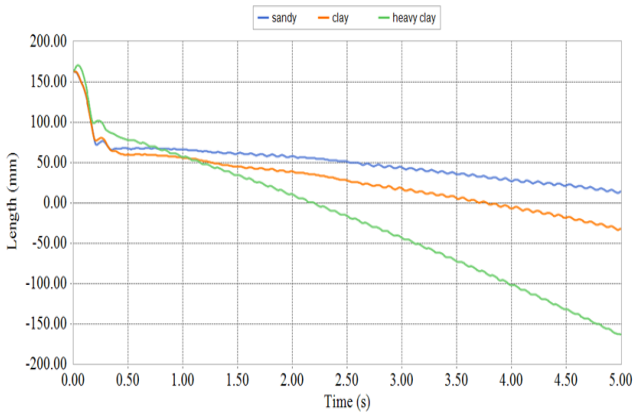

a

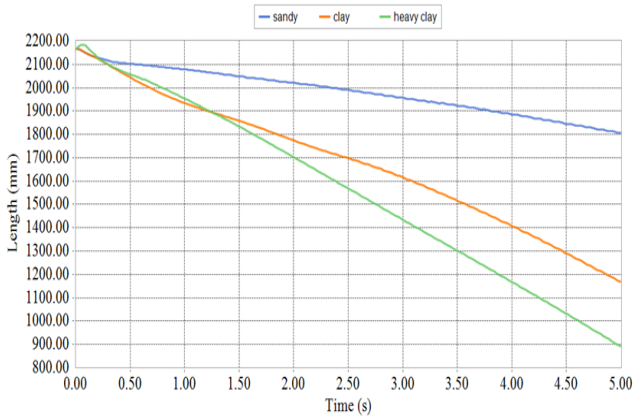

b

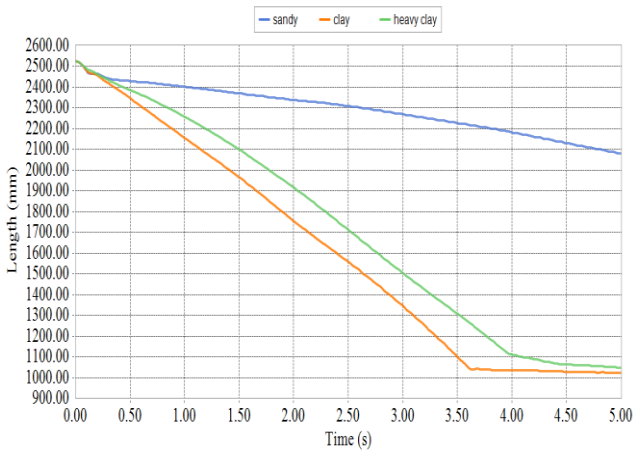

c

Fig. 22 Offset diagram when driving on a lateral ramp: a – 15°, b – 25°, c – 30°

The track chassis underwent simulations on three types of road surfaces, yielding the curve depicted in Fig. 24. Throughout the simulation, the track chassis successfully traversed a trench with a width of 400 mm but encountered difficulty with a width of 422 mm. The pitch angle of the chassis exhibited minimal fluctuation during the trench-crossing process, with fluctuations increasing alongside trench width. Notably, fluctuations were more pronounced on clay and heavy clay soils compared to sandy soil, indicating superior passability on sandy terrain. During traversal, the chassis maintained relatively stable speed on horizontal surfaces, with speed increasing when crossing the trench. Moreover, speed fluctuations escalated with trench width, with the most dramatic changes observed when traversing a 400 mm-wide trench, reaching peak values. Specifically, on sandy terrain, the chassis attained lower speeds compared to sticky and heavy sticky soils, with the most substantial speed variations occurring during 400 mm trench crossings. Speed changes on sandy soil were notably more consistent than on the latter two surfaces. While theoretically driven in a straight line, practical scenarios induce deviation. Analysis reveals similar offsets on sand and clay roads, with heavy clay roads exhibiting greater offsets. In conclusion, the track chassis' maximum trench-crossing width is 400 mm, with optimal passability observed on sandy surfaces.

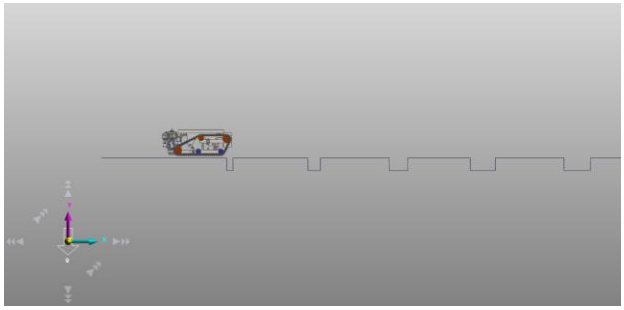

Fig. 23 Simulation of continuous chassis crossing trench

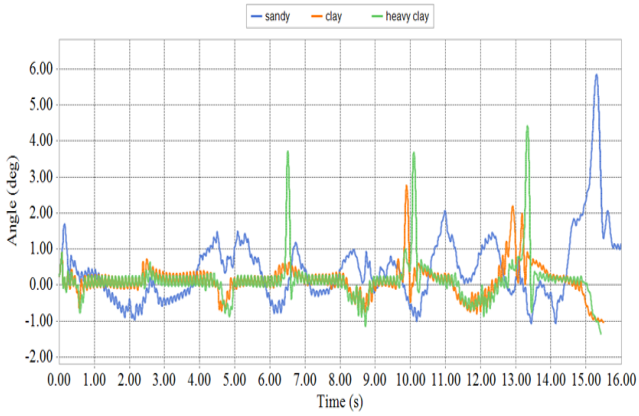

a

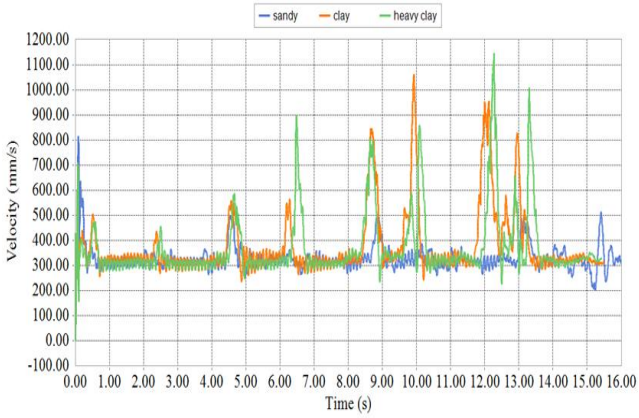

b

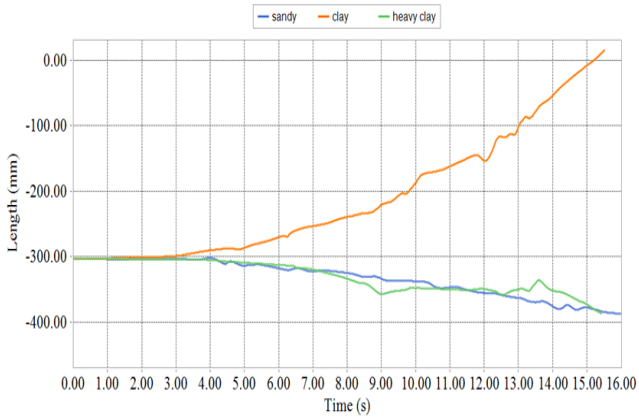

c

Fig. 24 Ditch-crossing curve diagram: a – centroid pitch angle diagram, b – centroid velocity diagram, c – travel offset diagram

4.3. Simulation analysis of obstacle crossing performance

The obstacle performance of the track chassis denotes its capacity to traverse the tallest obstacle at a consistent speed without toppling. This ability is typically contingent on soil type, obstacle height, driving speed, and centroid position. Utilizing RecurDyn, simulations were conducted across three pavement types-sandy soil, clay, and heavy clay-featuring obstacles of varying heights. Illustrated in Fig. 25, the obstacle crossing height is set at 150 mm. For the 150 mm vertical obstacle, the angular velocity driving function is STEP (time, 0.1,0,1.5, -13) for the driving wheel, the displacement driving function STEP (time, 0.1,0,3,80) + STEP (time, 3,0,4, -80) is set for the front hydraulic cylinder, and the displacement driving function STEP (time, 0.1,0,3, -80) + STEP (time, 3,0,4,80) is set for the rear hydraulic cylinder. The simulation time is 5 s and the number of steps is 3000 steps.

During the second stage of the obstacle crossing process, the pitch angle of the crawler chassis gradually increases until it reaches the third stage, signifying the successful traversal of the obstacle and smooth navigation on the road surface, as depicted in Fig. 26, a. The fluctuation in centroid pitch angle on both sand and clay road surfaces remains minimal, while on heavy clay terrain, it surpasses the former two surfaces, albeit remaining within acceptable limits to prevent overturning. Throughout the driving phase, the speed of the track chassis exhibits relative stability, peaking during the second stage of obstacle traversal alongside the maximum pitch angle. Notably, the speed required for overcoming vertical obstacles on heavy clay terrain exceeds that on sand and clay surfaces. Furthermore, as illustrated in Fig. 26, c, the longitudinal translation of the center of mass increases by 150 mm when traversing a vertical obstacle with a height of 150 mm. Simulation results indicate that the crawler chassis can effectively manage obstacles up to 150 mm in height without encountering overturning issues. However, obstacles exceeding 150 mm may cause overturning due to excessive pitch angles, with superior performance observed on sand and clay surfaces compared to heavy clay terrain.

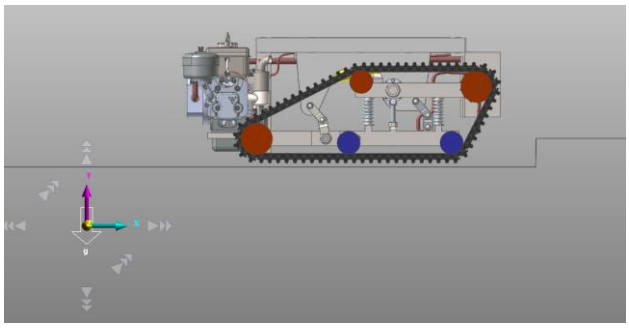

Fig. 25 Simulation of chassis obstacle crossing

Through the above analysis, it can be seen that the maximum speed of the tracked vehicle is about 1.3 m/s, which is basically consistent with the theoretical speed, so the validity of the model is verified.

5. Result Discussion

This paper presents an analysis and design of a miniature track universal chassis with adaptive terrain,

employing RecurDyn software to simulate the chassis's performance across climbing, trench-crossing, and vertical obstacle scenarios on three distinct terrains: sand, clay, and heavy clay. Results indicate superior performance on sand roads compared to clay and heavy clay surfaces. During climbing, chassis speed gradually diminishes with increasing slope, underscoring the critical role of climbing speed for optimal traversal performance. While higher speeds generally enhance performance, perpetual speed increases are constrained by chassis size and weight considerations. On transverse ramps, chassis offset is influenced by gravitational forces, notably lesser on sandy terrain compared to clay and heavy clay surfaces due to sand's tendency to compact. Hence, optimizing transverse slope performance necessitates careful consideration of chassis weight. In trench crossing stages, factors influencing maximum ditch width include chassis size, weight, and driving speed. Increased speed facilitates smoother traversal, albeit hindered by potential front-end subsidence, necessitating prudent weight management. Similarly, during vertical obstacle crossing, chassis angle gradually increases until reaching a critical tipping point. To prevent overturning, the approaching angle must not exceed the maximum pitch angle, warranting adjustments in chassis gap to accommodate larger obstacles. Simulation results affirm the miniature crawler chassis' commendable traversal performance and stability across diverse scenarios, underscoring its adaptability and versatility. Nonetheless, further research considerations include optimizing the center of gravity position to enhance overall performance, accounting for chassis weight and payload considerations.

Affected by the space, this paper mainly studies the structure, trafficability and stability of the micro adaptive terrain chassis. The adaptive performance is not elaborated in detail. The adaptive ability of this paper mainly refers to the adjustment of the attitude of the chassis through four lifting mechanisms. When driving on the longitudinal ramp, by controlling the expansion of the hydraulic cylinder, the two lifting mechanisms on the front side are reduced, while the two lifting mechanisms on the back side are increased, and the frame attitude is controlled. Backward, the center of gravity of the chassis moves forward, making it more conducive to climbing. When driving on the horizontal ramp, the two lifting mechanisms on the left side are reduced, and the lifting mechanism on the right side is raised, so that the right side of the chassis posture is raised, and the left side is reduced, so that the center of gravity moves to the left side, and the roll angle is reduced. When driving on the uneven ground, the control system controls the action adjustment of the four lifting mechanisms to change the posture and prevent the danger of overturning. The adaptive ability is multifaceted and suitable for many terrains. In general, the four lifting mechanisms cooperate with each other, which can realize the change of the ground clearance or angle of the chassis, and adjust in the direction of being conducive to passing in order to adapt to different environments.

In the future, the existing structure should be improved, the strength of the key structure should be checked, and the chassis should be further designed through theoretical analysis and simulation results. Therefore, the strength check and optimization of the chassis structure should be carried out in the future to make the chassis structure more reasonable and lightweight. The hydraulic system control system of the structure is studied in order to adjust the chassis posture in real time under different complex conditions and adapt to the change of terrain. Further research can be carried out on the intelligent technology of the chassis, such as remote control, autonomous navigation and path planning, task execution, intelligent control system, fault diagnosis and detection. And applied to agriculture, mining, rescue, military and other fields, and through continuous technological innovation and application expansion, intelligent track chassis will bring new challenges and opportunities for the development of various fields.

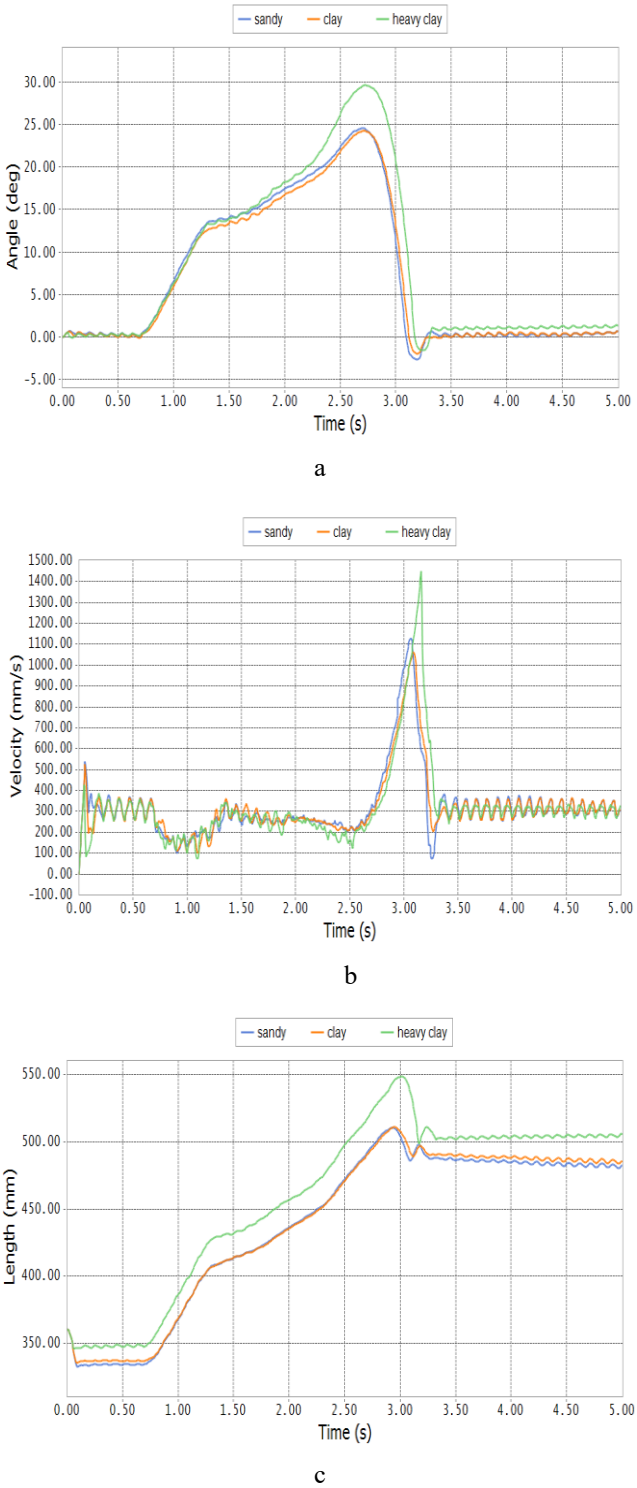

Fig. 26 Obstacle crossing curve diagram: a – centroid pitch angle diagram, b – centroid velocity diagram, c – centroid longitudinal translation diagram

6. Conclusions

1. Through a comprehensive analysis of the obstacle-crossing performance of the miniature general-purpose chassis navigating complex terrains, encompassing climbing longitudinal and lateral ramps, traversing vertical obstacles, and crossing trenches, a detailed force model governing the tracked chassis' dynamics during operation is established. This investigation elucidates the intricate relationship between the structural parameters of the tracked chassis and its traversal capabilities. Results reveal a maximum climbing angle of 36.99°, a peak lateral climbing angle of 34°, a maximum trench width tolerance of 422 mm, and an obstacle height clearance of up to 170 mm. Furthermore, a comprehensive analysis utilizing three-dimensional surface diagrams illustrates the correlation between structural parameters and traversal efficacy indices. Ultimately, it is deduced that factors such as driving slope, velocity, chassis configuration, track-ground adhesion coefficient, and centroid position play pivotal roles in determining the overall trafficability of the tracked chassis.

2. Utilizing SolidWorks, a comprehensive three-dimensional model of the crawler chassis is meticulously constructed, subsequently simulated via RecurDyn software. The simulation yields crucial curves depicting the centroid pitch angle, centroid velocity, bearing wheel pressure, roll angle, and offset over time. Remarkably, the results demonstrate the capability of the tracked chassis to navigate a longitudinal ramp with a steep inclination of 35°, while also negotiating a transverse ramp with a gradient of up to 30° without succumbing to rollover. Moreover, the chassis showcases its proficiency in traversing a trench measuring 400 mm in width and overcoming vertical obstacles reaching heights of 150 mm. Furthermore, the analysis underscores the superior trafficability of the chassis on sandy terrains compared to clay and heavy clay surfaces.

3. The simulation outcomes reveal that during climbing maneuvers, an advantageous configuration entails a forward and lower positioning of the center of gravity. Moreover, minimizing both the height of the center of gravity and its distance from the central axis of the chassis, while maximizing the gauge, enhances the chassis' performance. Similarly, when navigating trenches and vertical obstacles, positioning the center of gravity optimally facilitates overcoming such impediments.

4. A versatile micro-track chassis with adaptive terrain capabilities has been meticulously designed. It incorporates an attitude adjustment device, enabling the chassis to finely tune its posture and enhance ground clearance, thereby bolstering its overall traversing capability. Furthermore, serving as a robust bearing mechanism, the chassis can accommodate various devices and execute tasks across diverse scenarios. The synthesis of theoretical analysis and simulation research demonstrates that both methodologies yield results with an error margin of less than 10%, affirming the chassis' commendable passability. As a versatile carrying mechanism, it finds application across a spectrum of domains including robotics, UAV landing systems, medical equipment, military operations, industrial automation, and beyond.

Acknowledgements

Fund Project: National Natural Science Foundation of China. Project Name: Research on three-dimensional vision reconstruction and path planning method of mine intelligent shotcrete robot. Project Number: 52374156.

Fund Project: Major Science and Technology Projects in Anhui Province. Project Name: Adaptive terrain of hilly mountain micro agricultural machinery general chassis. Project Number: 2023a02020012.

References

1. **Eskandarian, A.; Wu, C.; Sun, C.** 2021. Research Advances and Challenges of Autonomous and Connected Ground Vehicles, IEEE Transactions on Intelligent Transportation Systems 22(2): 683-711. https://doi.org/10.1109/tits.2019.2958352.
2. **Rahman, M. M.; Ishii, K.;Noguchi, N.** 2019. Optimum harvesting area of convex and concave polygon field for path planning of robot combine harvester, Intelligent Service Robotics 12(2): 167-179. https://doi.org/10.1007/s11370-018-00273-4.
3. **Tang, S.; Yuan, S.; Hu, J.; Li, X.; Zhou, J.; Guo, J.** 2017. Modeling of steady-state performance of skid-steering for high-speed tracked vehicles, Journal of Terramechanics 73: 25-35. https://doi.org/10.1016/j.jterra.2017.06.003.
4. **Zhou, X.; He, J.; He, Q.; Ren, C.; Bhushan; He, M.** 2020. Motion Kinematics Analysis of a Horse Inspired Terrain-Adaptive Unmanned Vehicle With Four Hydraulic Swing Arms, IEEE Access 8: 194351-194362. https://doi.org/10.1109/access.2020.3033148.
5. **Wang, P.; Wang, S.; Jierula, A.; Wen, Z.** 2021. Automatic Identification and Location of Tunnel Lining Cracks, Advances in Civil Engineering 2021: 8846442. https://doi.org/10.1155/2021/8846442.
6. **Szrek, J.; Jakubiak, J.; Zimroz, R.** 2022. A Mobile Robot-Based System for Automatic Inspection of Belt Conveyors in Mining Industry, Energies 15(1): 327. https://doi.org/10.3390/en15010327.
7. **Aracri, S.; Giorgio-Serchi, F.; Suaria, G.; Sayed, M. E.; Nemitz, M. P.; Mahon, S.; Stokes, A. A.** 2021. Soft Robots for Ocean Exploration and Offshore Operations: A Perspective, Soft Robotics 8(6), 625-639. https://doi.org/10.1089/soro.2020.0011.
8. **Hutter, M.; Leemann, P.; Hottiger, G.; Figi, R.; Tagmann, S.; Rey, G.; Small, G.** 2017. Force Control for Active Chassis Balancing, IEEE/ASME Transactions on Mechatronics 22(2): 613-622. https://doi.org/10.1109/tmech.2016.2612722.
9. **Moghaddam, B. M.; Chhabra, R.** 2021. On the guidance, navigation and control of in-orbit space robotic missions: A survey and prospective vision, Acta Astronautica 184: 70-100. https://doi.org/10.1016/j.actaastro.2021.03.029.
10. **Li, H.; Mu, X.; Geng, D.; Yao, Y.; Wu, J.** 2022. Study and Experiment on the Operational Adaptability of Slope Corn Harvesters, Engenharia Agrícola 42(6): e20210230. https://doi.org/10.1590/1809-4430-eng.agric.v42n6e20210230/2022.
11. **Ugenti, A.; Galati, R.; Mantriota, G.; Reina, G.** 2023. Analysis of an all-terrain tracked robot with innovative suspension system, Mechanism and Machine Theory 182: 105237. https://doi.org/10.1016/j.mechmachtheory.2023.105237.

12. **Li, Y.; Zang, L.; Shi, T.; Lv, T.; Lin, F.** 2021. Design and Dynamic Simulation Analysis of a Wheel–Track Composite Chassis Based on RecurDyn, World Electric Vehicle Journal, 13(1): 12. https://doi.org/10.3390/wevj13010012.
13. **Zhou, Y.; Ding, Z.; Ding, D.; Xu, Y.; Yang, X.; Li, Z.; Cai, Y.; Sun, S.** 2022. Spatial Kinematic Analysis of a Tracked Forest Fire Engine with Fish-Bellied Swing Arm Torsion Bar Suspension, Applied Sciences 12(21): 11198. https://doi.org/10.3390/app122111198.
14. **Bai, Y.; Sun, L.; Zhang, M.** 2022. Design and analysis of multistage adaptive lateral deformation tracked robot, Journal of Mechanical Science and Technology 36(1): 371-383. https://doi.org/10.1007/s12206-021-1236-2.
15. **Wang, Z.; Ma, W.; Wang, T.; Liu, C.** 2022. Body Leveling Control Model Establishment and Experiment Analysis, Applied Engineering in Agriculture 38(2): 243-251. https://doi.org/10.13031/aea.14501.
16. **Hu, K.; Zhang, W.; Qi, B.** 2021. Analysis and design of auto-adaptive leveling hydraulic suspension for agricultural robot, International Journal of Advanced Robotic Systems, 18(5): 17298814211040634. https://doi.org/10.1177/17298814211040634.
17. **Wang, Z.; Yang, J.; Liu, P.; Long, X.; Li, H.; Wei, W.** 2019. Development of an agricultural vehicle levelling system based on rapid active levelling, Biosystems Engineering 186: 337-348. https://doi.org/10.1016/j.biosystemseng.2019.08.002.
18. **Andronov A.; Bacherikov, I.; Zverev, I.** 2021. Analysis of Platform Leveling Systems for Tracked Feller-Buncher Machines, Inventions 6(4): 96. https://doi.org/10.3390/inventions6040096.
19. **Xiao, J.; Wang, Y.; Li, X.; Zheng, J.** 2021. Design of high precision mechatronic-hydraulic leveling system for vehicle-mounted radar, Journal of Physics: Conference Series 2113(1): 012041. https://doi.org/10.1088/1742-6596/2113/1/012041.
20. **Yang, H.; Xia, C.; Han, J.; Chen, C.; Zhang, H.** 2020. Model and dynamic performance analysis of mountain tractor suspension implements, IOP Conference Series: Earth and Environmental Science 508(1): 012194. https://doi.org/10.1088/1755-1315/508/1/012194.

C. Su, H. Huang

ENHANCING TERRAIN ADAPTABILITY OF MICRO TRACKED CHASSIS: A STRUCTURAL DESIGN AND PERFORMANCE EVALUATION

S u m m a r y

Mobile robots operating in complex terrains demand superior traversability and adaptability. This study addresses this challenge by introducing a novel micro-tracked chassis design with improved terrain adaptability. The design utilizes track chassis as the bearing mechanism and optimizes its structure for improved performance. A combined approach involving theoretical analysis (e.g., mechanical calculations) and RecurDyn software simulations is employed to evaluate the cassis's ability to traverse various obstacles, including longitudinal and transverse slopes, trenches, and vertical barriers. The analysis reveals key performance metrics, showing a maximum climbing angle of 35°, a maximum side slope of 30°, a maximum trench crossing width of 400 mm, and a maximum surmountable vertical obstacle height of 150 mm. Furthermore, simulations across different soil types (sand, clay, and heavy clay) indicate superior passability on sandy terrain. Additionally, a forward-shifted center of mass configuration improves obstacle crossing performance and driving stability. This research offers valuable insights and a theoretical foundation for the design of micro tracked chassis with exceptional off-road capabilities

Keywords: track chassis, ramp, obstacle crossing, passability, RecurDyn.

Received April 4, 2024
Accepted December 16, 2024